NJC

Accepted Manuscript

This is an *Accepted Manuscript*, which has been through the Royal Society of Chemistry peer review process and has been accepted for publication.

Accepted Manuscripts are published online shortly after acceptance, before technical editing, formatting and proof reading. Using this free service, authors can make their results available to the community, in citable form, before we publish the edited article. We will replace this *Accepted Manuscript* with the edited and formatted *Advance Article* as soon as it is available.

You can find more information about *Accepted Manuscripts* in the Information for Authors.

Please note that technical editing may introduce minor changes to the text and/or graphics, which may alter content. The journal's standard Terms & Conditions and the Ethical guidelines still apply. In no event shall the Royal Society of Chemistry be held responsible for any errors or omissions in this *Accepted Manuscript* or any consequences arising from the use of any information it contains.

ROYAL SOCIETY OF CHEMISTRY

www.rsc.org/njc

The Synthesis of SnO_2/In_2O_3 Hetero-nanotubes by Coaxial-Electrospinning Method for Enhanced Formaldehyde Response

Jiuyu Liu, Xin Li, Xiang Chen, Hao Niu, Xiao Han, Ting Zhang, Huiming Lin*, Fengyu Qu*

College of Chemistry and Chemical Engineering, Harbin Normal University, P. R. China, Harbin 150025

Corresponding author: Tel/Fax: +86 0451 88060653.

E-mail address: qufengyu@hrbnu.edu.cn and linhuiming@hrbnu.edu.cn

Abstract

SnO_2/In_2O_3 hetero-nanotubes (SINs) were successfully produced by using a novel coaxial-electrospinning method with pure polyvinylpyrrolidone (PVP) plus Sn/In salt as the outer shell and PVP as the inner. After the calcination process, these SnO_2/In_2O_3 hetero-nanotubes with 80-120 nm in diameter and several micrometers in length were obtained. All SINs are assembled by plenty of nanoparticles (10-50 nm), bringing about abundant porous structure as well as large surface area (up to 56 m^2/g). These SnO_2/In_2O_3 hetero-nanotubes exhibit the high response (400 at 500 ppm), low detection limit (down to 250 ppb), fast response (60 s)/recovery (97 s), and well retentivity (94.68 % for 30 day) and selectivity toward formaldehyde. And the gas sensing mechanism has been discussed by adjusting the amount of the two components. Based on the detail investigation, the enhanced response performance lies in the particle size, porous structure, surface area, and component ratio of the heterostructure.

Keywords: SnO_2/In_2O_3; hetero-nanotubes; coaxial-electrospinning; formaldehyde; gas sensor

1. Introduction

With the industrial development, the air pollutions have become more and more serious. Therefore, gas sensors, especially towards hazardous/toxic gas, with effective, accurate and convenient performance are crucial. Currently, gas sensors based on metal-oxide semiconductors (WO_3, SnO_2, TiO_2, ZnO, and In_2O_3)[1-9] have attracted much attention, showing numerous significant potential superiorities, including low cost, fast sensitive, reusable, and simple to use etc.[10-15] Among the numerous metal oxides, indium oxide (In_2O_3), a typical n-type semiconductor with extremely significant wide-band-gap (3.55-3.75 eV), has been widely used in microelectronic areas including optical and electrical devices, solar cells, liquid-crystal displays[16-20], and ultrasensitive gas sensors[21-28].

Thus far, numerous In_2O_3 nanostructures, such as nanocrystals, nanoflowers, nanobelts, and nanospheres have been prepared using various methods and their sensitive behaviors have been investigated in detail. Chen et al. synthesized novel needle-like and flower-like In_2O_3 nanobundles via hydrolysis method, showing enhanced ultraviolet scattering and ethanol sensing[29]. Wang et al. successfully prepared porous In_2O_3 hollow spheres by a template-assisted method using Cu_2O as the sacrificial template, revealing the fast response towards acetone[30]. In addition, the doping in In_2O_3 nanomatrials is regarded as an efficient and simple way to enhance the gas-sensing properties. Currently, metal oxide (ZnO, Fe_2O_3, SnO_2), carbon (graphene, carbon nanotube, carbon nanofibers), noble metal (Pt, Pd, Ag), and element (N, Eu, Co) have been adopted in In_2O_3 to reduce the operating temperature and the response/recovering time, and to increase the selectivity.

Formaldehyde yet is used in many construction materials, and the volatilizable formaldehyde has become one of the most common indoor air pollutants. Furthermore,

formaldehyde is highly toxic to all animals. Long-term exposure an atmosphere rich in formaldehyde can be linked to an increased risk of respiratory illness, even of cancer. So, it is significant to develop the sensitive sensor to monitor formaldehyde so as to carry out the timely measures. In_2O_3-based sensors always have a low threshold of sensitivity to reducing gases and can operate in the ppm range[31]. In addition, SnO_2 nanoparticles are also the frequently applied sensing materials which have been used to fabricate reducing gas sensors. Furthermore, SnO_2/In_2O_3 nanocomposites possess many boundary of n–n hetero-junction, and the nanocrystallites boundary barrier of which may decreases when the composite materials meet reducing gas, and more electrons transfer from the gas to the sensing materials. Therefore, SnO_2/In_2O_3 nanocomposites are expected to reveal the enhanced response performance for formaldehyde detecting.

With high length-to-diameter ratio and ultra large special surface area, the 1D nanostructures, including nanofibers and nanotubes, have shown some honorable characteristics in sensor. Electrospinning technique was affirmed to be a versatile, effective, simple and low-cost method to fabricate 1D nano-structures. Herein, we present the fabrication of SnO_2/In_2O_3 (1D) nanotubes by using a coaxial-electrospinning method as shown in Scheme 1. The precursor in the outer syringe is composed of In and Sn salts, polyvinylpyrrolidone (PVP), and N, N-dimethylformamide (DMF), and the inner syringe is filled with PVP and DMF. Under the electrospinning process, the primary fibers were obtained on the aluminum foil with the volatilization of DMF. And then, the calcination treatment removes the organic component and also induces the decomposition and oxidation of the inorganic source to cause SnO_2/In_2O_3 nanotubes at last. Considering the novel nanostructure, these SnO_2/In_2O_3 nanotubes were adopted as sensors to detect formaldehyde, showing

the excited performance.

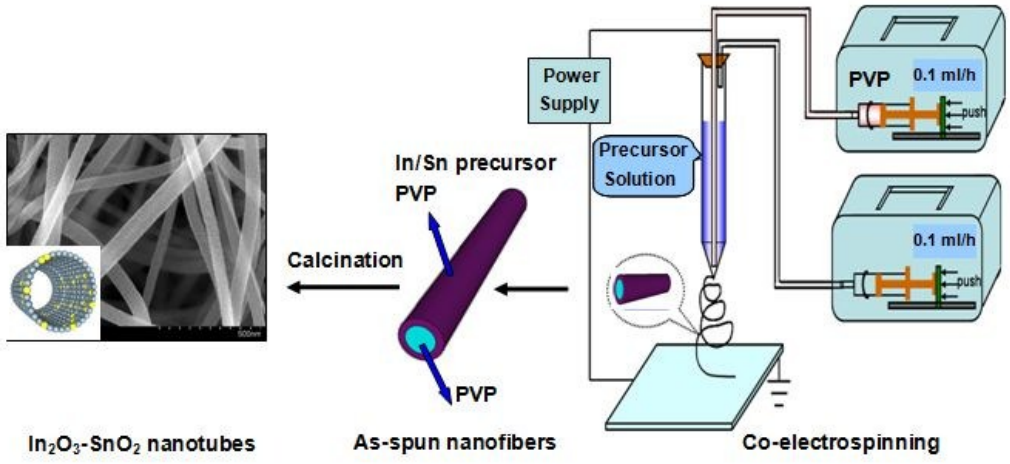

Scheme 1 Possible formation mechanism of SINs.

2. Experimental

2.1. Materials

Polyvinylpyrrolidone (PVP, Mw=1,300,000) and stannous chloride ($SnCl_2 \cdot 2H_2O$) were purchased from Aladdin. N, N-dimethylformamide (DMF) was bought from Tianjin Guangfu Chemical Co. (China). Indium nitrate ($In(NO_3)_3 \cdot 4.5H_2O$) was purchased from Sinopharm Chemical Reagent Co., Ltd. All the reagents were of analytical grade and used without further purification.

2.2. Preparation of SnO_2/In_2O_3 hetero-nanotubes

A suitable amount of $SnCl_2 \cdot 2H_2O$ and 0.2 g of $In(NO_3)_3 \cdot 4.5H_2O$ were added into 4 g of DMF. After being stirred for 2 h, 0.6 g of PVP was added into it and stirred for another 2 h. During coaxial electrospinning, the as-prepared precursor solution was loaded into the syringe as outer fluid and the inner fluid was the DMF (4 g) solution of PVP (0.75 g). The coaxial-electrospinning consists of the high voltage DC power supply, composite nozzles, the fluid supply system and the collecting board. The fluid speed was controlled by fluid supply system and the speed of the inner and outer fluid

was 0.1 ml/h. In this experiment, a voltage of 15 KV and a collection distance of 15 cm were applied for coaxial electrospinning. Then the primary fibers were calcined at 350 °C for 1 h， and then 600 °C for 3h in air to remove organic constituents and convert the precursor into nanocrystals. The sample with 0.05 g, 0.1 g and 0.15 g of $SnCl_2 \cdot 2H_2O$ was named SINs 0.05, SINs 0.1 and SINs 0.15, respectively.

2.3. Fabrication and Measurement of sensors

A moderate amount of SINs porous nanotubes were slightly grinded together with several drops of distilled water in an agate mortar. The formed paste was coated onto the electrode whose sides made by sliver. There were several sliver wires on the electrode to form a network pathway. Finally, the sensors were aged 12 h for test.

The gas sensing texts were conducted by a CGS-1TP intelligent gas sensing analysis system (Beijing Elite Tech Co., Ltd., China). The test gas was injected into the chamber (18 L in volume) using a syringe. The gas response was defined as S=Ra/Rg, where the Ra and Rg are the resistances of samples in air and the target gas. The response time is defined as the time required for the resistance to reach 90 % of the equilibrium value following an injection of the test gas, and the recovery time is the time necessary for the resistance to return to 10 % above original resistance in air after the removal of the test gas.

2.4. Characterization

The crystalline phase of the synthesized samples was determined by X-ray powder diffraction (XRD, Rigaku Dmax-rB, Cu Ka radiation, λ= 0.1542 nm 40 KV, 100 mA). The nitrogen adsorption/desorption was measured using a Micromeritics ASAP 2010M sorptometer. Specific surface areas and pore size distributions were calculated using the Brunauer-Emmett-Teller (BET) and Density Functional Theory (DFT) models from the adsorption branches, respectively. The morphology of the product

was examined by scanning electron microscopy (SEM, Hitachi-4800) and transmission electron microscopy (TEM, JEOL 2010EX).

3. Results and discussion

3.1. Material characterization

As shown in scheme 1, the nanotube structure is derived from the lack of inorganic composite in the inner part of the primary fibers. And the efficacy of inner PVP was investigated by varying the PVP amount in the inner syringe with the constant component in outer syringe (Fig. 1). From Fig. 1a, with 0.6 g of PVP in the inner syringe, the incomplete hollow fibers are obtained. The increase of the inner PVP to 0.75 g induces the uniform nanotube structure (Fig. 1b, known as SINs 0.1). Go on increasing it to 0.9 g, these tubes reveal the larger diameter (up to 150-200 nm) with shorter length because the remove of the too much inner PVP brings up the partial collapse of the hollow structure (Fig. 1c). As shown in Fig. 1, the appropriate inner PVP is significant for the formation of the uniform nanotube structure by the coaxial-electrospinning method.

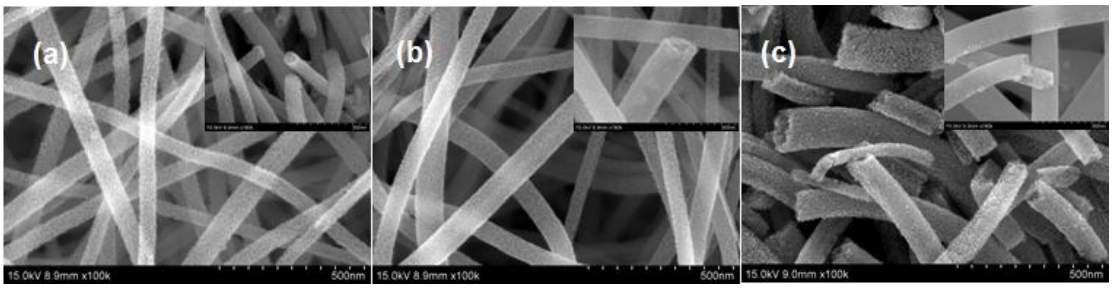

Fig. 1 SEM images of SINs with different weight of inner PVP: (a) 0.6g PVP, (b) 0.75g PVP, and (c) 0.9g PVP.

Moreover, the structure of SINs 0.1 was further studied by TEM. As displayed in Fig. 2a, SINs 0.1 possesses uniform nanotube structure with several micrometers in length, about 100 nm of the outer size and 50 nm of the inner size. From the high magnified TEM image (Fig. 2b), it can be found that SINs 0.1 are composed of many nanoparticles about 10 nm in size. These gaps of the accumulational nanoparticles bring abundant porous structure in SINs 0.1. From the high-resolution TEM image of SINs 0.1 (in Fig. 2c), the interplanar distance of 0.29 nm is closed to the lattice spacing of the (222) plane of the cubic phase In_2O_3 and the interplanar distance of 0.34 nm is ascribed to the (110) plane of the tetragonal rutile SnO_2. Furthermore, Fig. 2d and Fig. 2e show the STEM image and the EDS line scan analysis results correspond to the red line in Fig. 2d. From Fig. 2d, In, Sn and O elements are present along the compositional line and share a similar intensity trend, indicating the homogeneous dispersion of In, Sn and O in the nanotubes that is helpful for the electron transition between In_2O_3 and SnO_2. Moreover, there are sunk distributions for the atomic composition, which is in good accordance with the hollow structure as shown in the STEM and TEM images (Fig. 2c and Fig. 2d).

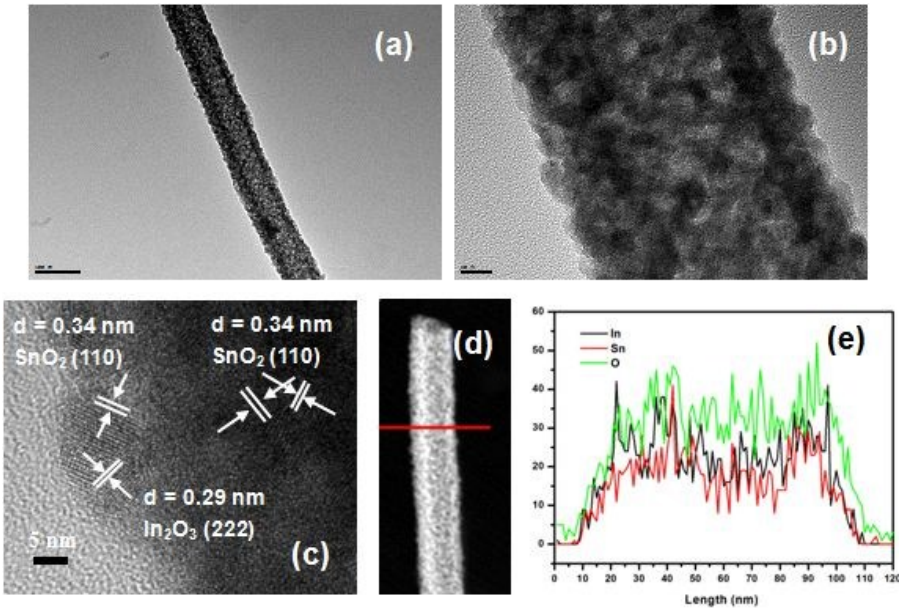

Fig. 2 TEM (a-c) images of SINs 0.1, (d) STEM image of a single fiber, (e) compositional line profiles across the fiber along the line as marked by the red line in (d)**.**

In addition, the SnO_2 amount also was varied and the corresponding SEM images of SINs 0.05 and SINs 0.15 are shown in Fig. 3. From Fig. 3**,** SINs 0.05 and SINs 0.15 also exhibit the similar nanotube structure as SINs 0.1 assembled by many crystallized In_2O_3 and SnO_2 nanoparticles (Fig. 3c, e, and f). However, when the Sn precursor is increased to 0.15 g, SINs 0.15 reveals some larger particles size up to 50 nm. And their crystalline structures were further studied by XRD, and the XRD patterns of curve a-c, corresponding to SINs 0.05, SINs 0.1, and SINs 0.15 are shown in Fig. 4. From Fig. 4, all samples reveal the typical diffractions of cubic phase In_2O_3 (JCPDS card no. 06–0416) and tetragonal phase SnO_2 (JCPDS card no. 41-1445). And no other peaks could be found indicating their purity. Furthermore, as the increase of the amount of Sn source, the diffraction strength of SnO_2 increases owing to the larger particle size with enhanced crystalline degree of SnO_2 nanocrystallites. In addition, the diffraction peaks of In_2O_3 is widened with the doping of SnO_2, implying the decrease of the particle size of In_2O_3.

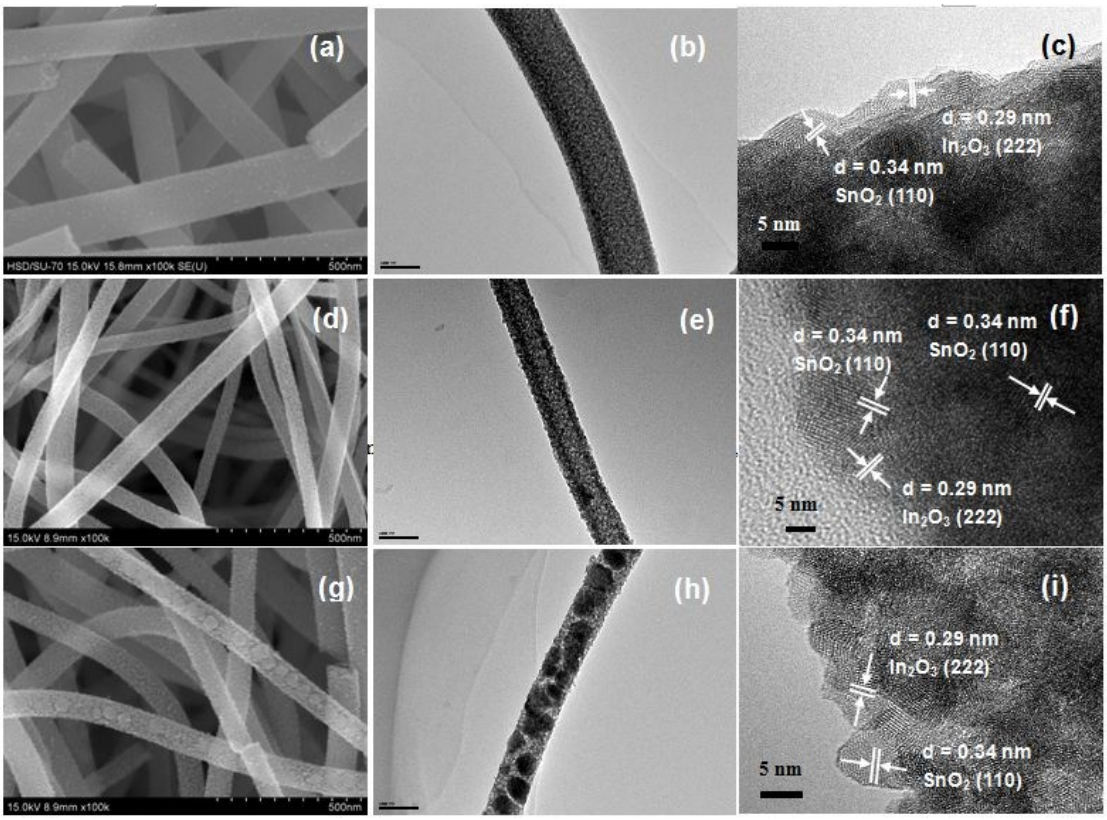

Fig. 3 SEM and TEM images of SINs 0.05 (a-c), SINs 0.1 (d-f), and SINs 0.15 (g-i).

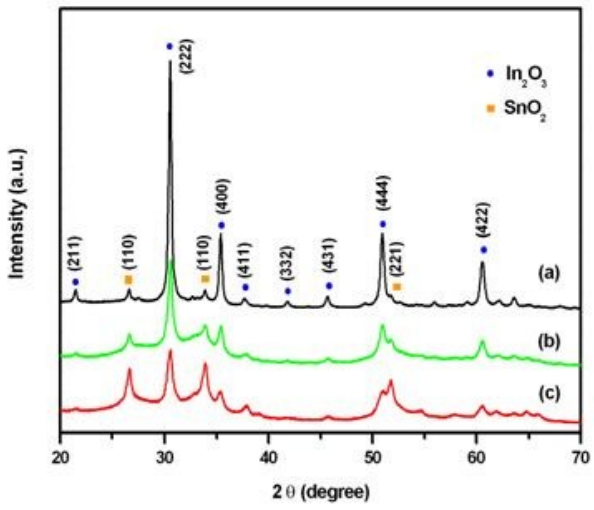

Fig. 4 XRD of patterns of (a) SINs 0.05, (b) SINs 0.1, and (c) SINs 0.15.

Moreover, the degradation and oxidation process also were studied by TG-DSC analysis. Fig. 5a, b and c exhibit the TG-DSC of primary fibers of SINs 0.1 (a) In/PVP (b), and Sn/PVP (c). The obvious loss weight at 250-350 °C is mainly considered as the degradation and oxidation of organic component (PVP). The next loss weight beyond 350 °C is ascribed to the oxidation of the inorganic component. From Fig. 5a, the primary fibers of SINs possesses the DSC exothermic peak centering at 484 and 565 °C owing to the oxidation of In and Sn precursor, respectively. Based on the previous reports, the degradation/oxidation of organic component (before 400 °C) produces plenty of gases, such as CO_2 and steam etc, that generates a pressure difference between the inner and the outside of the nanofibers to cause these inorganic nanoparticles tend to outside and to insure the formation of the nanotube structure.

The porous structures of the SnO_2/In_2O_3 nanotubes were also analyzed by nitrogen adsorption isotherm techniques. Fig. 6 presents the nitrogen adsorption-desorption isotherms and BJH pore size distribution curves of all samples. As observed in Fig. 6a, all SnO_2/In_2O_3 nanocomposites exhibit the type IV isotherms with H_3 hysteresis loops at middle relative pressure region (P/P_0 = 0.4-0.8), implying the split porous structure originated from the accumulation of nanoparticles that agrees well with the result of TEM. The corresponding pore size distribution curves were obtained by the BJH method as displayed in Fig. 6b. SINs 0.1 displays the pore size distribution centering at 3.4 and 6.8 nm and that of SINs 0.05 and SINs 0.15 is 6.8 nm and 3.4, 4.4 nm, respectively. With the abundant porous structure, all samples display large surface area and pore volume to be 29 m^2/g and 0.081 cm^3/g, 45 m^2/g and 0.089 cm^3/g, 56 m^2/g and 0.096 cm^3/g for SINs 0.05, SINs 0.1, and SINs 0.15, respectively (Table 1). As mentioned above, with the increase of Sn precursor, more nanoparticles are present to build the more porous structure, which is constructed by

the accumulation of the nanopaticles to induce the increased surface area.

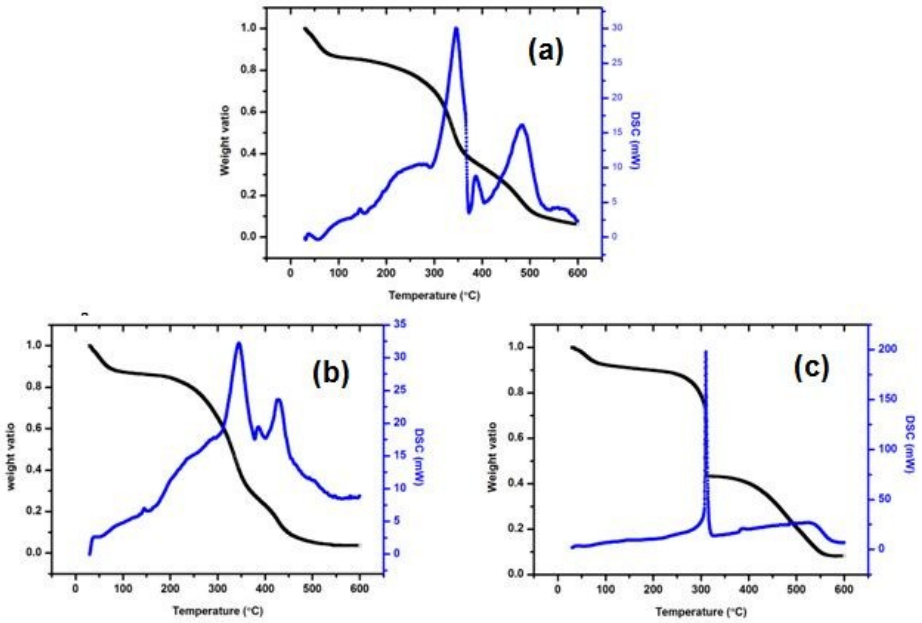

Fig. 5 Thermal gravimetry-differential scanning calorimetry (TG-DSC) curves of the primary SINs 0.1 (a), In_2O_3 NTs (b) and SnO_2 NTs (c).

Sample	BET surface area (m^2/g)	Pore volume (cm^3/g^{-1})	Pore diameter (nm)
SINs 0.05	29	0.081	6.8
SINs 0.1	45	0.089	3.4 6.8
SINs 0.15	56	0.096	3.4 4.4

Table 1 The porous parameters of all samples.

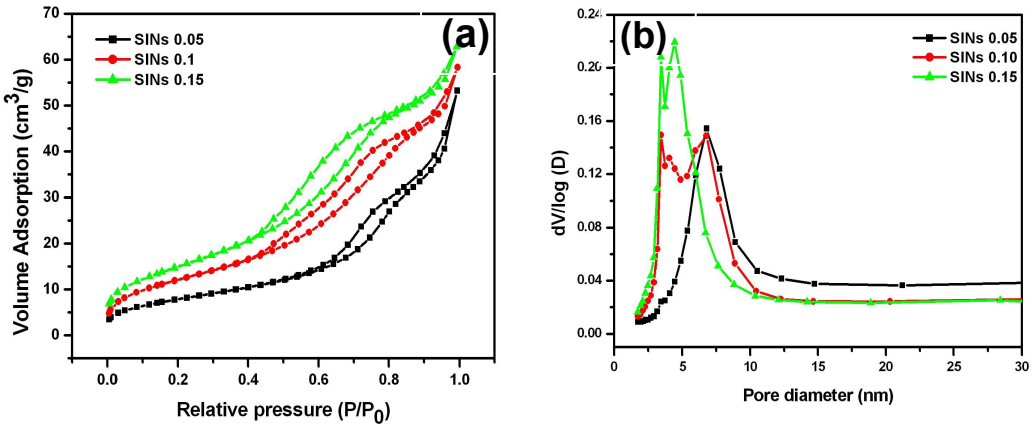

Fig. 6 N_2 adsorption–desorption isotherms (a) and BJH pore size distribution (b) of the samples.

3.2. Gas sensing properties

Considering the excellent hetero-nanotube structure, SINs were adopted as the sensor for formaldehyde detecting. Firstly, the optimum operating temperature is investigated. Fig. 7 gives the responses of these sensors based on SINs 0.05, SINs 0.1 and SINs 0.15 versus operating temperature with formaldehyde concentration of 50 ppm. As displayed in Fig. 7, with the increase of the operating temperature, the response increases as well. When the temperature increases to 300 °C, the response (Ra/Rg) of SINs 0.05, SINs 0.1, and SINs 0.15 reaches 18.5, 118, and 42, respectively. Further increasing the temperature, the response decreases obviously. Therefore, 300 °C is chosen to be an operating temperature for further response test.

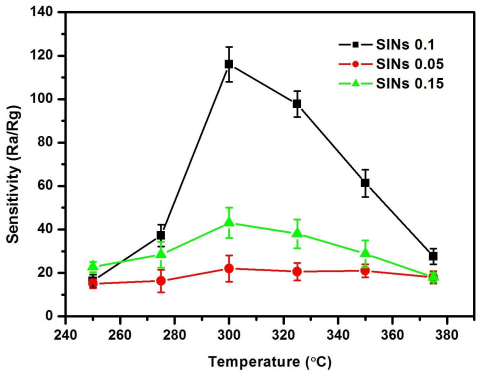

Fig. 7 The response of SINs 0.05, SINs 0.1, and SINs 0.15 sensor to 50 ppm HCHO at different operating temperature.

Fig. 8 shows the response of SINs 0.05, SINs 0.1 and SINs 0.15 towards various concentrations of formaldehyde (10-500 ppm). From Fig. 8, all samples reveal the sensitive response toward the formaldehyde. With increasing of formaldehyde concentration, the response increases obviously. When the formaldehyde

concentration increases to 500 ppm, the response reaches 57, 400, and 360 for SINs 0.05, SINs 0.1, and SINs 0.15, respectively. The excellent response of these nanostructues owing to the novel 1D nanotube structure, nanoparticle size and porous structure, which facilitate the fast gas molecule transfer on to the surface of the inner nanoparticles to enhance the response[43]. Moreover, the highest response of SINs 0.1 is ascribed to the small particle size (10 nm in size) and large surface area. However, with the largest surface area (56 m^2/g), SINs 0.15 does not reveal the highest response of all. So it is believed that besides surface area the In/Sn ratio also plays a significant part in the response. As revealed in Fig. 8, the combination of In_2O_3 and SnO_2, SINs systems reveal the improved response than the pure In_2O_3 or SnO_2 nanotubes. It is known that, the boundary between SnO_2 and In_2O_3 nanoparticles is an n–n homotype hetero-junction, and the nanocrystallites boundary barrier of which may decreases when the composite materials meet formaldehyde, and more electrons transfer from the gas to the sensing material, and so the response of the sensor increases[32-34]. The comparison of sensing performance with the previous reports has been summarized in Table 2. From Table 2, SINs 0.1 also displays a rather excellent response compared with the reported In_2O_3-based sensors[35-42].

	Materials	**Synthesis method**	**Morphology**	**Response (Ra/Rg) 50 ppm HCHO**	**Ref.**
1	SnO_2/In_2O_3	Electrospinning	Nanotubes	118	here
2	SnO_2	Solvothermal	Nanospheres	15	34
3	In_2O_3	Hydrothermal	Microbundles	4.2	35
4	SnO_2/InO_3	Electrospinning	Nanofibers	18.9	36
5	$Cdln_2O_4$	Hydrothermal	Octahedrals	24	37
6	Zn-In_2O_3	Hydrothermal	Hollow spindles	14	38
7	In_2O_3	Hydrothermal	nanorod-flower	40	39
8	In_2O_3	Solvothermal	Hollow spheres	6	40
9	In_2O_3	Nanocasting Route	Nanorods	50	41
10	In_2O_3	Template	Nanowire-like	45	42

Table 2 The comparison of sensing performance with the previous reports.

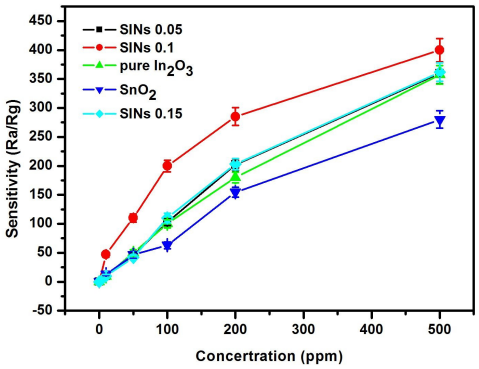

Fig. 8 The response of SINs 0.05, SINs 0.1, SINs 0.15, pure In_2O_3 nanotubes and pure SnO_2 nanotubes to HCHO.

In addition, the response and recovery of SINs 0.1 sensor to different concentrations of formaldehyde are also exhibited in Fig. 9. From Fig. 9a, when formaldehyde was injected, the response fast reaches the equilibrium. And after the atmosphere was removed the response recovered to the initial soon. The response and recovery time at 50 ppm is calculated to be 60 s and 97 s (including the diffusion time), respectively. The fast response and recovery might be attributed to the nanoparticle size and large surface area which provides a small dimension for effective electron transport and chemical reaction[31-32]. From Fig. 9, the response increases as the gas concentration increasing. With the concentration of formaldehyde at 10, 50, 100, 200 and 500 ppm, the corresponding response is about 46.9, 118, 202.5, 288, and 404, respectively. Furthermore, the response of SINs 0.1 toward formaldehyde below 5 ppm also was studied. From Fig. 9b, SINs 0.1 also reveals 9 (5 ppm), 3 (1 ppm), 1.65 (500 ppb), 1.44 (250 ppb) response. From the response curve of SINs 0.1 to formaldehyde, the response can be divided into three sections that are 250 ppb-5 ppm, 5-100 ppm, and 100-500 ppm section and their corresponding linear

relationship were surveyed, respectively. From Fig. 10b-c, the high R value of every liner matching confirms the well liner relationship that is significant in the practical application for the gas sensor.

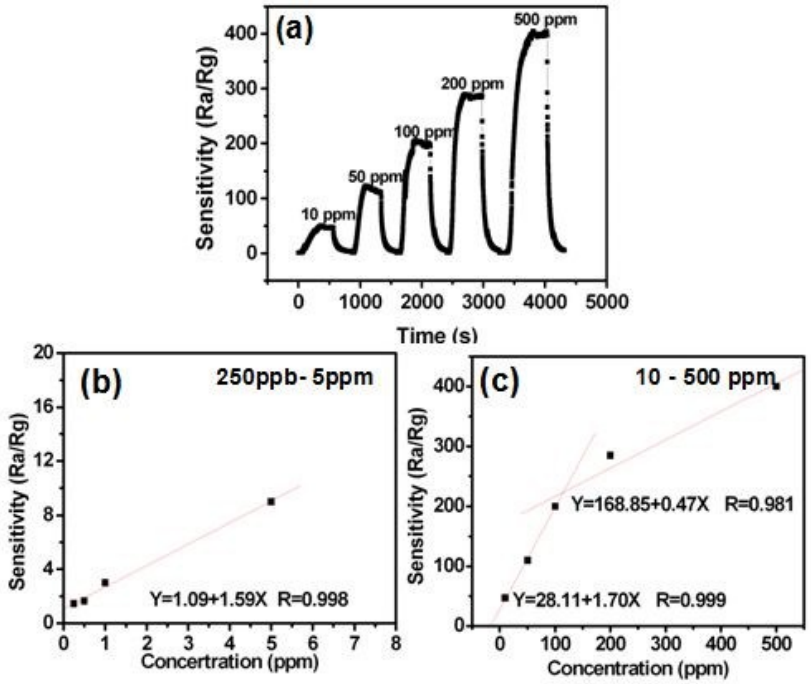

Fig. 9 (a) The response and recovery characteristic of SINs 0.1 sensor to formaldehyde (10-500 pmm). (b) and (c) The linear relationship of the response to concentration.

Besides the response, the selectivity of these sensors is another important indicator to evaluate the sensors. Fig. 10 shows the bar graph of the response of SINs 0.05, SINs 0.1, and SINs 0.15 to various gases with the concentration of 50 ppm. As displayed in Fig. 10, SINs 0.1 also reveals the highest response to HCHO (118), and the response to NO, ethanol, acetone, toluene, CO, methanol, benzene, and SO_2 is 68, 10.5, 4.6, 3, 2.9, 2.4, 1.8, and 1.44, respectively. It can be found that the response to HCHO is almost 1.73 times higher than NO and above 10 times for the others. The excellent selectivity is significant for the practical application of SINs 0.1 to be used in HCHO sensor. Moreover, SINs 0.1 sensor also exhibits the considerable stability for formaldehyde detect even for 30 days. From Fig.11, after 30 days, the response of SINs 0.1 sensor also can remain 94.68 % response as the initial. From the above

investigation, SINs 0.1 possesses high response, low detection limit, fast response/recovery, and well recycle ability and selectivity, showing the well potential application on formaldehyde sensor.

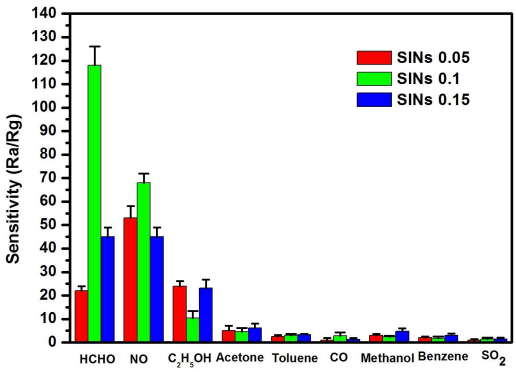

Fig. 10 Selectivity of the SINs 0.1 sensor to 50 ppm various gas.

3.3. The gas sensing mechanism of the SnO_2/In_2O_3 hetero-nanotubes

On the basis of the above results, the sensing mechanism of porous metal oxide based sensors can be explained as follows: when the sensing materials are in air, oxygen molecules will be adsorbed on the sensor surface to produce negatively charged chemisorbed oxygen species, which are formed by capturing electrons from the conductance band. As a result, the chemisorbed oxygen species will act as surface acceptors, trapping electrons and increasing surface resistance of the nanosensor. As the target reducing gases were injected, they would react with the formed oxygen ions and the trapped electrons would then be released back to the sensing materials surfaces, resulting in a drastic decrease of the resistance of n-type materials (SnO_2 and In_2O_3). Therefore, the capability to adsorb oxygen molecules is crucial to improve the gas-sensing performance.

$$1/2\ O_2 + e^- \rightarrow (O_2^-)_{ads} \qquad (1)$$

$$(O_2^-)_{ads} + e^- \rightarrow 2(O^-)_{ads} \qquad (2)$$

When n-type material meets reducing formaldehyde, the possible reaction might

be preceded as following[43]:

$HCHO_{(g)} + O^-_{ads} \rightarrow CHOOH_{(g)} + e^-$ (3)

The reactions produce electrons, and the resistance of the sensors in formaldehyde vapor decreases. So the response, which was defined as S=Ra/Rg (Ra and Rg are the resistances of samples in air and the target gas), increases according to the increase of the concentration of formaldehyde.

4. Conclusion

In summary, SnO_2/In_2O_3 hetero-nanotubes were synthesized by a coaxial -electrospinning process with polyvinylpyrrolidone (PVP) and Sn/In salt solution as the outer shell and pure PVP solution as the inner. After the oxidation treatment, the pressure difference makes the hollow structures of these SnO_2/In_2O_3 hetero-nanotubes, which are assembled by plenty of nanoparticles to produce a mass of porous structure as well as large surface area (up to 56 m^2/g). With the novel nanostructure, SnO_2/In_2O_3 hetero-nanotubes reveal high response, low detection limit, fast response/recovery, and well recycle ability and selectivity, showing the well potential application on formaldehyde sensor. Under the above investigation, the particle size, porous structure, surface area, and component ratio of the hetero-structure can be used to adjust the response performance. Furthermore, the simple synthetic strategy also is expected to be used to prepare other semiconductor metal oxide or hetero-structure with various porous structure and large surface for some practical application, such as adsorption, catalyst, and photoelectricity, etc.

Acknowledgments

Financial support for this study was provided by the National Natural Science Foundation of China (21471041, 21171045, 21441002, 21571045), Natural Science Foundation of Heilongjiang Province of China ZD201214, and College Youth Innovation Talents Training Program UNPYSCT-2015053.

References

[1] X. F. Lu, X. C. Liu, W. J. Zhang, C. Wang, Y. Wei. Journal of Colloid and Interface Science. 2006, 298, 996-999.

[2] W. Zeng, C. N. Dong, B. Miao, H. Zhang, S. B. Xu, X. Z. Ding, et al. Materials Letters. 2014, 117, 41-44.

[3] X. H. Zhang, M. X. Huang, Y. J. Qiao. Materials Letters. 2013, 95, 67-69.

[4] Y. Zheng, J. Wang, P. Yao. Sensors and Actuators B-Chemical. 2011, 156, 723-730.

[5] Q. Z. Yu, M. Wang, H. Z. Chen. Material Letters. 2010, 64, 428-430.

[6] A. Walsh, J. L. F. D. Silva, S. H. Wei, C. Korber, A. Klein, L. F. J. Piper, A. DeMasi, K. E. Smith, G. Panaccione, P. Torelli, D. J. Payne, A. Bourlange, R. G. Egdell. Physical Review Letters. 2008, 100, 167402 /1-167402/4.

[7] F. Zhou, X. Li, J. Shu, J. Wang. Journal of Photochemistry and Photobiology A-Chemistry.2011, 219, 132-138.

(8) E. Li, Z. Cheng, J. Xu, Q. Pan, W. Yu, Y. Chu. Crystal Growth Design. 2009, 9, 2146-2151.

[9] S. K. Lim, S. H. H. Wang, D. Chang, S. Kim. Sensors and Actuators B-Chemical. 2010, 149, 28-33.

[10] J. Polleux, A. Gurlo, N. Barsan, U. Weimar, M. Antonietti, M. Niederberger. Angewandte Chemie International Edition. 2006, 45, 261-265.

[11] J. J. Chen, K. Wang, L. Hartman, L. W. Zhou. Physical Chemistry Chemical Physics. 2008, 112, 16017-16021.

[12] L. Francioso, L. M. A. Taurino, A. Forleo, Siciliano, P. Sensors and Actuators B-Chemical. 2008, 130, 70-76.

[13] J. Zhang, R. S. Wang, M. Y. Wang, Y. Wang, L. B. Zhu, J. H. Xia, Z. X. Guo, M. S. Zhang, P. W. Huang, H. S. Wu. Sensors and Actuators B-Chemical. 2009, 135, 610-617.

[14] G. Neri, A. Bonavita, G. Micali, G. Rizzo, E. Callone, G. Carturan. Sensors and Actuators B: Chemical. 2008, 132, 224-233.

[15] J. H. Lee. Sensors and Actuators B: Chemical. 2009, 140, 319-336.

[16] D. H. Zhang, C. Li, S. Han, X. L. Liu, T. Tang, W. Jin, C. W. Zhou. Applied Physics Letters. 2003, 82, 112-114.

[17] C. G. Granqvist. Applied Physics A-Solids and Surfaces. 1993, 57, 19.

[18] Y. Shigesato, S. Takaki, T. Haranoh. Journal of Applied Physics. 1992, 71, 3356-3364.

[19] A. Gurlo, M. Ivanovskaya, N. Bârsan, M. Schweizer-Berberich, U. Weimar, W. Göpel, A. Diéguez. Sensors and Actuators B: Chemical. 1997, 44, 327-333.

[20] M. Liess. Thin Solid Films. 2002, 410, 183-187.

[21] N. Singh, C. Y. Yan, S. P. Lee. Sensors and Actuators B: Chemical. 2010, 150, 19-24.

[22] G. Korotcenkova, A. Cerneavschia, V. Brinzaria, A. Vasilieva, M. Ivanova, A. Cornetb, J. Moranteb, A. Cabotb, J. Arbiolb. Sensors and Actuators B: Chemical. 2004, 99, 297-303.

[23] J. Tamaki, C. Naruo, Y. Yamamoto, M. Matsuoka. Sensors and Actuators B: Chemical. 2002, 83, 190-194.

[24] H. Y. Lai, T. H. Chena, C. H. Chen .Sensors and Actuators B-Chemical. 2001, 76, 639-643.

[25] T. Hyodo, H. Inoue, H. Motomur, K. Matsuo, T. Hashishin, J. Tamaki, Y. Shimizu, M. Egashira. Sensors and Actuators B: Chemical. 2010, 151, 265-273.

[26] S. H. Wei, Y. Yu, M. H. Zhou. Materials Letters. 2010, 64, 2284-2286.

[27] J. Moona, J. A. Park, S. J. Lee, T. Z. yung, I. D. Kim. Sensors and Actuators B: Chemical. 2010, 149, 301-305.

[28] Y. H. Li, J. Gong, G. H. He, Y. L. Deng. Synthetic Metals. 2011, 161, 56-61.

[29] H. Y. Lai, T. H. Chena, C. H. Chen .CrystEngComm. 2012, 14, 5589-5595.

[30] D. Han, P. Song, H. Zhang, Z. Yang, Q. Wang. Materials Letters. 2014, 124, 93-96.

[31]. H. Yamaura, K. Moriya, N. Miura and N. Yamazoe, Sensors and ActuatorsB. 2000, 65, 39.

[32] A. Kolmakov, D. O. Klenov, Y. Lilach, S. Stemmer, M. Moskovits. Nano Letters. 2005, 5, 667-673.

[33] A. Kolmakov, M. Moskovits. Annual Review of Materials Research. 2004, 34, 151-180.

[34] W. Wang, Z. Y. Li, W. Zheng, H. M. Huang, C. Wang, J. H. Sun. Sensors and Actuators B: Chemical. 2010, 143, 754-758.

[35] Z. Li, Q. Zhao, W. Fan and J. Zhan. Nanoscale. 2011, 3, 1646-1652.

[36] Z. Li, H. Yan, S. Yuan, Y. Fan, J. Zhan. Journal of Colloid and Interface Science. 2011, 354, 89-93.

[37] H. Du, J. Wang, M. Su, P. Yao, Y. Zheng, N. Yu. Sensors and Actuators B: Chemical. 2012, 20, 166-167.

[38] Y. Liu, C. Kong, X. Lü, F. Liao, F. Huang, J. Lin. Crystal Growth & Design. 2012, 14, 4104-4108.

[39] Z. He, Z. Chen, Y. Li, Q. Zhang, H. Wang. CrystEngComm. 2011, 13, 2557.

[40] Y. Fan, S. Wang, Z. Sun. Materials Chemistry and Physics. 2012, 134, 93–97.

[41] P. Song, W. Zhang. Materials Research Bulletin. 2014, 53, 177–184.

[42] S. Yi, S. Tian, D. Zeng, K. Xu, S. Zhang, C Xie. Sensors and Actuators B: Chemical. 2013, 185, 345-353.

[43] J. Wang, P. Zhang, J. Q. Qi, P. J. Yao. Sensors and Actuators B: Chemical. 2009, 136, 399-404.

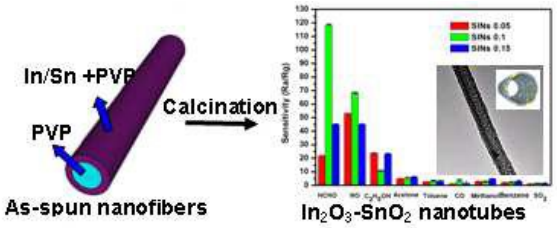

SnO_2/In_2O_3 hetero-nanotubes were successfully produced by using coaxial-electrospinning method to exhibit high sensitivity and fast response/recovery toward formaldehyde.